The AAPS Journal (2019) 21: 63
DOI: 10.1208/s12248-019-0338-6

Check for updates

Research Article

In Vitro Metabolism and Hepatic Intrinsic Clearance of the Synthetic Cannabinoid Receptor Agonist JWH-122 and Its Four ω-Halogenated Analogues

Anders Bork Davidsen,[1] Marie Mardal,[1,2] and Kristian Linnet[1]

Received 20 March 2019; accepted 28 April 2019; published online 15 May 2019

Abstract. The number of new psychoactive substances (NPS) emerging on the illicit drug market has increased over the last decade. Halogenation of existing illicit drugs is a particular trend, with the purpose of both circumventing the law and altering the toxicodynamic and toxicokinetic profiles of the compounds. This study investigates the *in vitro* impact of JWH-122 ω-halogenation (fluoro, chloro, bromo and iodo) on the metabolism, apparent intrinsic hepatic clearance and analytical targets for detecting drug consumption. Metabolite profiling was conducted with pooled human liver microsomes, suspended rat hepatocytes and pooled human hepatocytes. The *in vitro* half-life was also determined in pooled human hepatocytes. All samples were analysed by liquid chromatography/high-resolution mass spectrometry. All compounds, except for JWH-122, showed high formation rates of phase I metabolites, predominantly ω-COOH and methylnaphthyl hydroxylation metabolites. Phase II metabolites were ω-*O*-glucuronides, methylnaphthyl *O*-glucuronides and ω-glutathione conjugates. The relative ion intensity of the glutathione conjugates increased with the ω-halogen size, with I-JWH-122 having the highest intensity. Stability studies gave a low half-life and a high intrinsic hepatic clearance for JWH-122 (1305 mL/min/kg) and MAM-2201 (1408 mL/min/kg). Cl-, Br- and I-JWH-122 showed increasing half-life with increasing ω-halogen size, with intrinsic clearance values of 235–502 mL/min/kg. The recommended analytical targets for consumption of JWH-122 or ω-halogenated JWH-122 analogues are the ω-COOH metabolites for unspecific profiling and the methylnaphthyl hydroxylated metabolites to distinguish the compounds. Furthermore, ω-halogenation with larger halogens appears to increase the intrinsic hepatic stability, thereby prolonging exposure and possibly the duration of action.

KEY WORDS: synthetic cannabinoid receptor agonist; hepatocyte metabolism; microsome metabolism; high-resolution mass spectrometry; intrinsic hepatic clearance.

INTRODUCTION

Abuse of new psychoactive substances (NPS) has been on the rise in the last decade, and analytical targets in biological matrices are therefore required to identify drug consumption. One large group of NPS is formed by the synthetic cannabinoid receptor agonists (SCRA), which all have inherent CB_1 or/and CB_2 receptor activity. The number of NPS detections per year has recently stagnated, but SCRA remain the most seized NPS in Europe (1). The emerging SCRA consist of modifications that include halogenations, as observed in the case of JWH-122 where a hydrogen on the ω-carbon is substituted with a fluoride to yield MAM-2201. This fluorinated NPS has been detected in cases of fatal poisoning and intoxications (2,3). Substitutions with fluoride, as well as with larger halogens, have been observed with other NPS, including NBoMes (4), AM-2201, THJ-2201 and XLR-11 (5,6). These modifications of already-known compounds could alter the pharmacodynamics (7) and/or metabolic fate of the compounds, thereby giving rise to new analytical targets in biological samples.

Noble *et al.* (8) and Cannaert *et al.* (9) investigated the CB_1 and CB_2 receptor activity of JWH-122 and the fluoro, chloro, bromo and iodo ω-halogenated analogues of JWH-122. The halogen modification showed a half-maximal effective concentration (EC_{50}) ranging between 60.5 and 283.7 nM for CB_1 and 2.7 and 23.4 nM for CB_2. The addition

Electronic supplementary material The online version of this article (https://doi.org/10.1208/s12248-019-0338-6) contains supplementary material, which is available to authorized users.

[1] Section of Forensic Chemistry, Institute of Forensic Medicine, University of Copenhagen, Frederik V's Vej 11, Copenhagen, Denmark.
[2] To whom correspondence should be addressed. (e–mail: marie.mardal@sund.ku.dk)

of bromide and iodide reduced the CB_1 activity compared with JWH-122, while fluoro- and bromo-halogenation showed an increase and a reduction, respectively, in CB_2 receptor activity when compared with JWH-122. These studies indicate that halogenation of SCRA may affect the pharmacodynamic profile, while the activity variations indicate potential hazards or benefits of ω-halogenation of existing compounds. Notably, users report a shorter perceived half-life of NPS when compared with natural cannabis, thereby indicating altered pharmacodynamics and/or pharmacokinetic parameters (10).

The metabolic fate of NPS compounds following ingestion is essentially unknown. As a result, the use of *in vitro* metabolic systems, such as pooled human liver microsomes (pHLM), rat hepatocytes (RH) or pooled human hepatocytes (pHH), is required to identify human metabolic pathways. Furthermore, these *in vitro* systems can also be utilised to predict pharmacokinetic parameters. *In vitro* methods for clearance prediction were first described by Rane *et al.* in 1977 (11), and the methods have evolved since then to include other pharmacokinetic parameters, such as half-life and the unbound fraction. In general, several *in vitro* systems are available for kinetic and metabolic experiments and are used for *in vitro–in vivo* extrapolation. Each system has its own unique advantages and disadvantages regarding ease of handling, precision and *in vivo* representation of the data obtained (12–14). When no *in vivo* data are available for the compound of interest, the metabolic pathway and enzymes involved are often unknown. Therefore, the use of primary hepatocytes can be considered because of the *de novo* production of metabolic cofactors, as well as presence of non-CYP metabolic enzymes (15).

The aim of the present study was to investigate the impact of the substitution of different ω-halogens on the metabolism and intrinsic hepatic stability of SCRA, specifically JWH-122 analogues. The metabolism, half-life and intrinsic hepatic clearance were evaluated by *in vitro–in vivo* extrapolation (IVIVE) of JWH-122 and four of its ω-halogenated analogues shown in Fig. 1. *In vitro* metabolism studies were conducted by incubating the compounds in pHLM and/or RH and pHH and evaluating the products by high-resolution mass spectrometry.

MATERIALS AND METHODS

Chemicals and Reagents

JWH-122, JWH-122-D_{11}, ω-COOH-JWH-122-D_4, MAM-2201 and Cl-, Br- and I-JWH-122 were purchased from Chiron AS (Trondheim, Norway). JWH-018 was purchased from Lipomed (Arlesheim, Switzerland). 5F-APP-PICA was kindly donated from the European Response project (grant agreement number JUST/2013/ISEC/DRUGS/AG/6413). Cryopreserved RH (forward donors) were obtained from Fisher Scientific (Loughborough, UK). Cryopreserved pHH were purchased from BioNordika (Herlev, Denmark). Analytical grade methanol, acetonitrile, water and formic acid (> 99%) were purchased from Fisher Scientific (Loughborough, UK). Ammonium formate (> 99%) was purchased from Sigma Aldrich (St. Louis, MO, USA). Dimethyl sulphoxide (DMSO) anhydrous (> 99.8) was purchased from VWR Chemicals (PA, USA). Foetal bovine serum (FBS), Leibowiz's 15 medium and cryopreserved hepatocyte recovery medium were purchased from Fisher Scientific (Loughborough, UK). The NADPH regenerating system and pHLM were purchased from Corning Lifesciences (NY, USA). All other chemicals were of analytical grade or higher. All analytical compounds were dissolved in DMSO at concentrations of 1 mg/mL as working solutions. Hepatocytes were stored in liquid nitrogen.

In Vitro Metabolism Studies

Metabolite Profiling in pHLM

In vitro metabolism studies of all five compounds were conducted as described by Noble *et al.* (16). Briefly, microsomes (1 mg/mL) were preincubated for 10 min before the addition of the NADPH regenerating system consisting of $NADP^+$ (1.3 mM), glucose-6-phosphate (3.3 mM), $MgCl_2$ (3.3 mM), glucose-6-phosphate dehydrogenase (0.4 U/mL) and 0.05 mM sodium citrate. The JWH-122, MAM-2201 or Cl-, Br-, or I-JWH-122 were then added to a final concentration of 1 μM in 0.1 M phosphate buffer in a total volume of 250 μL (organic content < 0.5%). The incubations were stopped at time points 0 and 30 min by quenching 30 μL of the reaction mixture in 60 μL ice-cold acetonitrile containing internal standards JWH-018 and 5F-APP-PICA (100 ng/mL). The samples were centrifuged at 2000*g* at 4°C and stored at −20°C until analysis. As a control for NADPH-dependent metabolism, the NADPH cofactor was omitted and the volume was replaced with water.

Metabolite Profiling in Suspended Rat Hepatocytes and in Pooled Human Hepatocytes

Hepatocyte incubations for metabolite profiling were conducted in suspension with cryopreserved Wistar RH and cryopreserved pHH. Cl-, Br- or I-JWH-122 were incubated at concentrations of 10 μM in L-15 medium supplemented with 10% FBS at a viable cell density of 1 million cells/mL (organic content < 0.5%). Compounds were incubated for up to 3 h at 37°C at 150 rpm on a Thermomixer comfort (Eppendorf, Hamburg, Germany), and sampling was performed at 0, 1 and 3 h. Samples were quenched in ice-cold acetonitrile containing internal standards JWH-018 and 5F-APP-PICA (100 ng/mL). Quenched samples were centrifuged at 1000*g* for 10 min at 4°C and stored at −20°C until analysis. Diclofenac was used as a positive control at a concentration of 10 μM, as described by Wohlfarth *et al.* (17).

Intrinsic Hepatic Clearance Determination Using Primary Hepatocytes

Intrinsic hepatic clearance experiments were conducted with cryopreserved pHH for all five compounds, essentially as described by Soars *et al.* (18) but with some minor modifications. Compounds were incubated at a final concentration of 2 μM with an organic content below 1% (*v/v*). Two compound solutions (4 μM), each at volumes of 350 μL in L-15 medium, were produced without serum added to avoid

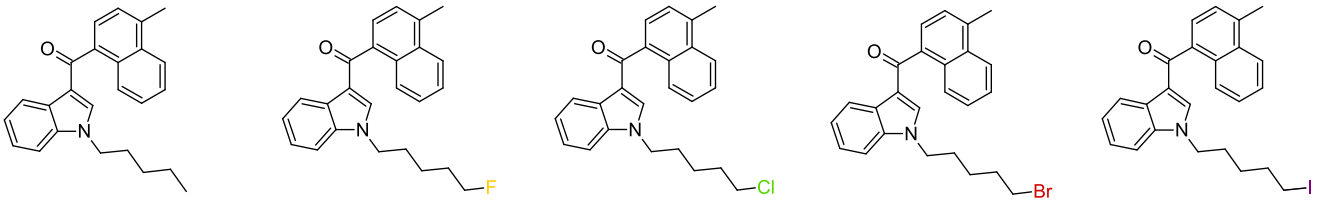

1: JWH-122 2: MAM-2201 3: Cl-JWH-122 4: Br-JWH-122 5: I-JWH-122

Fig. 1. Compounds investigated for metabolism and hepatic clearance

plasma protein binding. Two pHH vials, each containing 350 μL and 2 million cells/mL, were preincubated for 5 min in a water bath kept at 37°C. Reactions were initiated by mixing the 350 μL hepatocyte suspension with the 350 μL compound solution. Aliquots of 50 μL were removed in duplicate from the first vial at time points 0, 0.5, 1, 2, 3 and 6 min. From the second vial, aliquots were removed in duplicate at time points 15, 30, 45, 60, 75 and 90 min. Vials were periodically inverted to reduce hepatocyte sedimentation. All aliquots were immediately centrifuged at 7000*g* for 30 s using a Sigma 1-14 centrifuge (Sigma, Germany), and 30 μL of the supernatant was transferred to 90 μL ice-cold acetonitrile containing internal standards (JWH-122-D_{11} and JWH-122-COOH-D_4 100 ng/mL). Samples were frozen for at least 1 h at −20°C and centrifuged at 2000*g* for 20 min at 4°C. The supernatants were analysed as described below.

LC-MS Analysis

The samples were separated and analysed using a Dionex Ultimate 3000 liquid chromatography (LC) system (Thermo Scientific, Dionex Softron, Germering, Germany) coupled to a Q-exactive mass spectrometer (MS) (Thermo Fisher Scientific, Bremen, Germany) with a heated electrospray ionisation (HESI) source. The autosampler temperature was maintained at 5°C. The samples were separated with an Acquity HSS C18 1.8 μm, 2.1 × 150 mm column from Waters (Wexford, Ireland) maintained at 45°C and a flow rate of 0.310 μL/min. The mobile phases were mobile phase A (aqueous 2 mM ammonium formate with 0.1% *v/v* formic acid) and mobile phase B (acetonitrile with 0.1% *v/v* formic acid). Calibration was performed using an external calibration standard purchased from Thermo Fisher. Three different analytical methods were developed and applied for different parts of the study.

Metabolite Identification. Qualitative studies for metabolite profiling were conducted with a gradient from 25 to 99% of mobile phase B for 12 min, isocratic at 99% B for 2 min, and 1 min of equilibration at 25% B, for a total analysis time of 15 min per run. The injection volume was 5 μL. Positive MS detection was done in full MS with data-dependent detection ($ddMS^2$) in the range 200–700 *m/z*, with a resolution of 35,000, an automatic gain control (AGC) of 3e6 ions and a maximum injection (IT) time of 50 ms. The $ddMS^2$ analysis was conducted at resolution of 17,500, AGC 1e5, maximum IT 50 ms, and an isolation window of 1 *m/z*. The collision gas was nitrogen with a normalised collision energy (NCE) stepped at 17.5, 30 and 45 eV, with a spray voltage at 2.5 kV and a capillary temperature of 320°C. Negative ionisation was performed with similar parameter settings, except the scan range was 150–700 *m/z* and the maximum IT was 200 ms.

Metabolite Confirmation. Metabolite identities were confirmed using the LC settings and full MS parameters from the metabolite identification method. Targeted analysis was performed by full MS and parallel reaction monitoring (PRM) to improve mass spectral information for accurate metabolite identification. Full scan data were collected in the range 150–700 *m/z*. PRM detection was performed with an inclusion list consisting of maximum four compounds per analysis with the following positive and negative PRM settings: resolution 17,500, AGC target 2e5, maximum IT 100 ms, isolation window 1 *m/z* and a collision energy of 10, 30 and 50 eV.

Quantitative Characterisation. The quantitative method was developed for enhanced chromatographic separation of a selection of targets with a gradient elution from 50 B to 99% over 12 min. Quantifications were conducted in full MS all ion fragmentation (AIF). Full scan MS settings were set as positive ESI, resolution 35,000, AGC target 3e6 with a maximum IT 200 ms and a scan range between 200 and 700 *m/z*. AIF settings were at resolution 35,000, AGC 3e6, maximum IT 200 ms, scan range 100–700 *m/z* and a collision energy at 35 eV.

Data Analysis

The LC instrument was controlled by Xcalibur 4.0 (Thermo Scientific, USA). Tracefinder 4.1 forensic software (Thermo Scientific, USA) was used for quantification of obtained data, and metabolite identification was assisted by Compound Discoverer software (Thermo Fisher, USA).

Method validation was performed by investigating the linearity, limit of quantification (LOQ) and carryover. The linear range was ensured over six calibration levels of concentration covering lower LOQ (LLOQ) 0.001–3 μM for ω-COOH-JWH-122 and 0.1–3 μM for JWH-122 and the ω-halogenated analogues. Three samples at each concentration level were analysed over the course of 2 days. The calibrators were prepared in the same matrix composition as the samples. Accuracy was $< \pm 20\%$. Quality control (QC) samples were prepared at four levels (0.001, 0.1, 1 and 2.25 μM) and had a precision and CV% < 20%. The intermediate precision of the control samples at low levels (0.001 and 0.1 μM) and at the high level (3 μM) was below

20%. Calculations were performed with internal standard corrected areas using ω-COOH-JWH-122-D_4 for the metabolites and JWH-122-D_{11} for the analytes. The slope of the linear part of the natural logarithm of % drug remaining *versus* time plot was used as an expression of the elimination rate constant, *k*.

Toxicokinetic *in vitro–in vivo* extrapolation was performed using the procedure described by Obach (19).

$$T_{1/2} = \frac{0.693}{k} \tag{1}$$

$$CL'_{H,int} = \frac{0.693}{T_{1/2}} \cdot \frac{mL\ incubation}{hepatocytes} \times \frac{hepatocytes}{g\ liver} \times \frac{g\ liver}{kg\ body\ weight} \tag{2}$$

$$CL'_{H,int} = \frac{0.693}{T_{1/2}} \cdot \frac{0.7mL}{1 \times 10^6 cells} \times 99 \times 10^6 cells/g \times \frac{1799g}{70kg}$$

The *in vitro* half-life, $T_{½}$, is expressed in minutes and calculated from the elimination rate constant, Eq. 1. Upscaling to human organ intrinsic clearance, $CL'_{H,int}$, was performed using Eq. 2. The $CL'_{H,int}$ for a human liver was achieved by including the mL incubation per hepatocyte, with physiological scaling factors for hepatocytes from Poulin and Haddad in 2013 (20).

RESULTS AND DISCUSSION

The metabolites were identified by comparison of HR-MS/MS mass spectra and fragmentation patterns obtained from the parent compounds. PRM scans at three collision energies are presented in the Supplementary information for all identified metabolites.

Metabolite Identification Using LC-HR-MS/MS

Hydroxydiclofenac and diclofenac acyl glucuronide were observed in the diclofenac positive controls, thereby confirming phase I and phase II metabolic activity, respectively. Metabolite identification was performed based on $ddMS^2$, followed by metabolite confirmation by PRM. The metabolite mass-to-charge, retention time and fragment ions from the PRM scans after RH and pHH incubation are shown in Table I. In the present paper, the fragmentation and metabolite identification will only be discussed for Cl-, Br- and I-JWH-122, as the metabolites and metabolic pathway for JWH-122 and MAM-2201 have previously been investigated (21–23). Cl-, Br- and I-JWH-122 were observed with *m/z* 390.1619, 434.1140 and 482.0975, respectively. The Cl- and Br-JWH-122 presented with the characteristic isotopic ratio in full scan detection. The three compounds shared a common fragment ion of the methylnaphthyl moiety, giving rise to a fragment ion with *m/z* 169.0648. Furthermore, the indole moiety, in combination with the pentyl chain, gave rise to fragment ions *m/z* 248.0838, 292.0324 and 340.0199. Upon fragmentation at 50 eV, the indole fragment ion *m/z* 144.0445 was observed for all compounds (see Supplementary information). Characterisation and identification of detected metabolites were based on the characteristic *m/z* shifts from the parent compounds' fragmentation pattern and the chromatographic behaviour (see Fig. 2).

In total, nine metabolites (M1–M9) were detected in at least one of the three metabolic systems. The oxidative dehalogenated metabolite, M1, is observed with a shift of the indole-*N*-pentyl ion to *m/z* 230.1178, whereas the ω-carboxylated metabolite, M4, had an indole-*N*-pentyl fragment ion with *m/z* 244.0969 corresponding to the characteristic shift of the carboxylic acid. The fragment ion corresponding to a hydroxylation of the methylnaphthalene, M2, gave rise to a shift of the methylnaphthyl moiety to 185.0598 *m/z*. The dihydrodiol, M3, presented with a methylnaphthyl fragment ion with *m/z* 203.0705, which, after a loss of water, presented as *m/z* 185.0598. The indole and methylnapththyl dihydroxylated metabolite, M5, showed fragment ion *m/z* 185.0598 and the hydroxylated indole fragment ion with *m/z* 248.1088 and 364.0785 for MAM-2201 and Cl-JWH-122, respectively.

The metabolite M7, the *O*-glucuronidated phase II metabolite of M2, showed a loss of the glucuronide to M2 and further fragmentation to the already-described M2 metabolite fragment ion. The metabolite M8, originating from the *O*-glucuronidation of M1, showed a loss of the glucuronide and subsequent M1 fragmentation. The ω-glutathione-conjugated metabolite, M9, was observed in positive ionisation full MS with *m/z* 661.2693 and the characteristic methylnaphthalene fragment ion with *m/z* 169.0647. M9 was further confirmed in the negative ionisation mode and presented characteristic collision-induced dissociation fragment ions of GSH with *m/z* 272.0888, 210.0880 and 179.0451 (24).

Proposed Metabolic Pathways

Based on the detected metabolites, the metabolic pathway depicted in Fig. 3 is proposed for JWH-122 and its ω-halogenated analogues.

An initial metabolic step was the ω-hydroxylation or oxidative dehalogenation, resulting in the JWH-122-*N*-5-OH metabolite M1, which is in accordance with metabolic studies on JWH-122 and MAM-2201 (22). The following ω-carboxylation was observed for all compounds, giving the shared metabolite of JWH-122-COOH M4, likely *via* an aldehyde intermediate. Monohydroxylation of the methylnaphthyl moiety, M2, was observed for all investigated compounds. M6 is presumably an oxidation product from M4 and/or M2 and consists of both a monohydroxylated and a ω-carboxylated moiety for all compounds except JWH-122. The dihydrodiol formation on the methylnaphthyl moiety, M3, is likely obtained through epoxide formation with subsequent hydrolysis. M2 was further hydroxylated on the indole moiety, resulting in M5.

The phase 2 metabolic pathways include *O*-glucuronidation of the hydroxyl group of M1 and M2, resulting in the metabolites M8 and M7, respectively. The glutathione-conjugated metabolite, M9, is produced by

Table I. Metabolite Identification Scheme After up to 3 h of Incubation of Rat Hepatocytes and Pooled Human Hepatocytes. Accurate Masses Are Shown from Full MS and Product Reaction Monitoring Scans in pHH, 30 eV Normalised Collision Energy, and Obtained in Positive Mode, Unless Otherwise Specified. Data Is Not Shown for M5

ID	Name		*m/z* (ppm**)	Formula	RT	Compound specific fragment ion (*m/z*)		MS peak area, absolute intensity					
								RH			pHH		
								0 h	1 h	3 h	0 h	1 h	3 h
Phase I metabolites													
M1	Oxidative dehalogenation		372.1959 (0.27)	$C_{25}H_{25}NO_2$	8.20	169.0648, 230.1177	Cl	2.16E+06	1.40E+06	1.18E+06	1.81E+06	4.05E+06	5.58E+06
						169.0648, 230.1177	Br	1.76E+06	1.47E+06	1.58E+06	1.74E+06	1.45E+06	6.26E+06
						169.0648, 230.1177	I	5.15E+06	2.30E+06	1.16E+06	1.10E+07	1.19E+07	1.15E+07
M2	Methylnaphthalene hydroxylation	Cl	406.1570 (0.49)	$C_{25}H_{24}NO_2Cl$	8.25	185.0599, 248.0838	Cl	3.63E+06	3.16E+06	5.66E+06	1.72E+06	6.22E+06	1.15E+07
		Br	450.1068 (0.44)	$C_{25}H_{24}NO_2Br$	8.15	185.0598, 292.0328	Br	1.58E+06	2.04E+06	3.38E+06	2.99E+05	3.33E+05	3.81E+06
		I	498.0934 (2.00)	$C_{25}H_{24}NO_2I$	9.16	185.0602, 340.0200	I	2.32E+06	1.76E+06	1.55E+06	1.30E+06	2.46E+06	1.42E+07
M3	Dihydrodiol formation	Cl	424.1671 (0.71)	$C_{25}H_{26}NO_3Cl$	7.657.61	185.0598, 203.0706, 248.0840	Cl	1.78E+06	1.67E+06	3.27E+06	3.65E+04	2.47E+05	5.12E+05
		Br	468.1172 (6.19)	$C_{25}H_{26}NO_3Br$	7.48	185.0598, 203.0710, 292.0324	Br	3.54E+05	6.37E+05	1.30E+06	N/A	1.05E+04	1.77E+05
		I	516.1038 (1.55)	$C_{25}H_{26}NO_3I$		185.0600, 203.0709, 340.0199	I	4.34E+05	4.99E+05	5.08E+05	1.36E+04	5.87E+04	2.68E+05
M4	ω-COOH		386.1752 (0.26)	$C_{25}H_{23}NO_3$	7.88	169.0648, 244.0970		7.09E+06	5.75E+06	1.31E+07	3.29E+06	1.46E+07	2.69E+07
								3.23E+06	4.86E+06	1.22E+07	3.82E+06	6.23E+06	1.78E+07
								5.52E+06	5.90E+06	9.23E+06	1.54E+07	1.88E+07	3.05E+07
M6	ω - C O O H + methylnaphthalene hydroxylation		402.1702 (0.50)	$C_{25}H_{23}NO_4$	7.28	185.0598, 244.0969		7.43E+05	5.94E+05	1.42E+06	7.26E+04	2.43E+06	5.05E+06
								3.30E+05	5.05E+05	1.16E+06	1.44E+05	8.70E+05	6.04E+06
								1.64E+05	2.69E+05	4.20E+05	2.79E+05	8.03E+05	6.54E+06
Phase II metabolites													
M7	Methylnaphthalene *O*-glucuronide	Cl	582.1896 (1.20)	$C_{31}H_{32}NO_8Cl$	6.57	185.0596, 169.0652, 248.0841	Cl	1.24E+05	2.37E+05	4.38E+05	N/A	5.32E+05	1.31E+06
		Br	626.1390 (1.12)	$C_{31}H_{32}NO_8Br$	7.52	185.0597, 450.1066, 292.0349	Br	4.97E+04	8.09E+04	1.36E+05	N/A	8.50E+04	2.17E+06
		I	674.1254 (1.34)	$C_{31}H_{32}NO_8I$	7.96	185.0602, 340.0187, 498.0897	I	2.06E+03	1.20E+04	1.34E+04	9.61E+03	2.07E+05	4.15E+06
M8	ω-*O*-glucuronide		548.2283 (0.73)	$C_{31}H_{33}NO_8$	7.55	169.0648, 372.1959, 230.1183		2.58E+04	4.73E+04	8.32E+04	1.16E+04	8.61E+05	1.71E+06
								1.05E+05	1.07E+05	1.56E+05	2.59E+05	8.74E+05	3.67E+06
								9.72E+04	1.30E+05	1.49E+05	3.25E+05	1.01E+06	3.90E+06
M9	ω- GSH conjugation		661.2682 (1.06)	$C_{35}H_{40}N_4O_7S$	5.40	169.0647		1.56E+05	2.92E+05	7.51E+05	N/A	5.13E+04	1.12E+05
			659.2544*			272.0886*, 210.0880*,179.0455*		2.00E+07	3.21E+07	4.14E+07	4.91E+06	7.59E+06	1.07E+07
								1.61E+07	3.23E+07	3.72E+07	7.20E+06	7.08E+06	2.16E+07

ppm parts pr. million, *RT* retention time, *MS* mass spectrometric, *RH* rat hepatocytes, *pHH* pooled human hepatocytes
*Negative mode data dependent acquisition
**Mass error from peak apex in Trace Finder (Thermo Fisher)

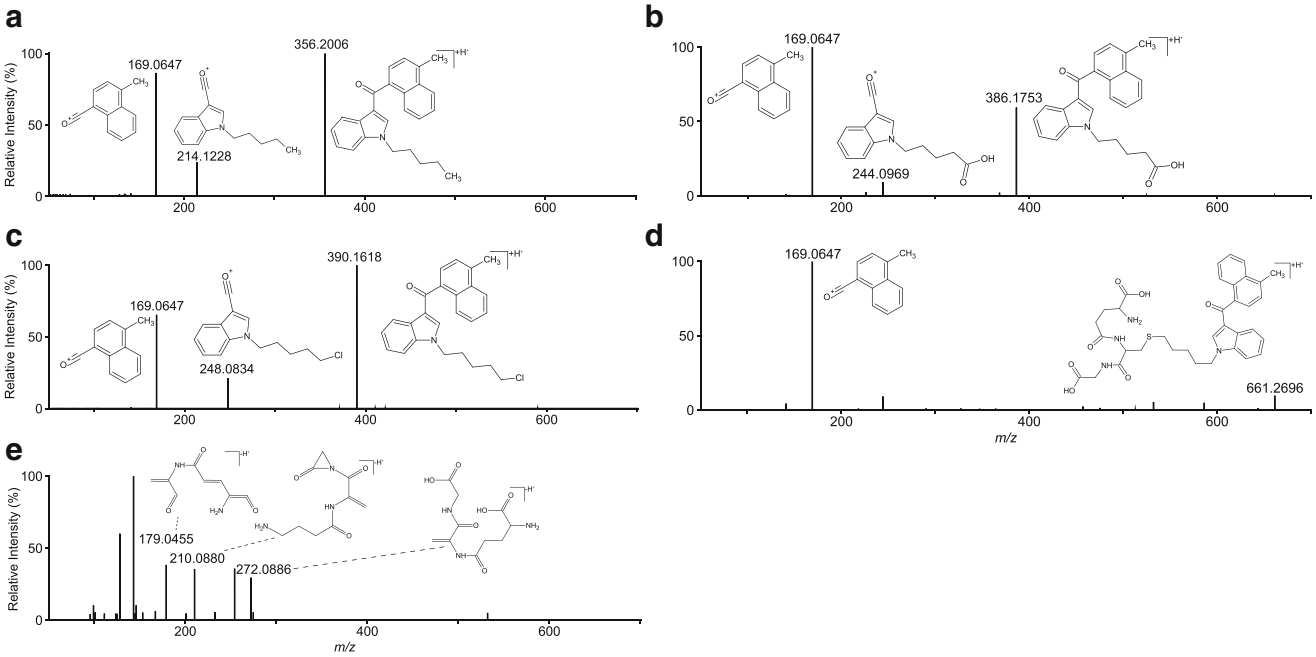

Fig. 2. ESI$^+$-HR-MS/MS spectra acquired after collision-induced dissociation with a NCE of 30 eV of **a** JWH-122, **b** M4, **c** Cl-JWH-122, **d** M9 and ESI$^-$-HR-MS/MS spectra of **e** M9

glutathione S-transferase with S_N2 displacement of the ω-halogen as observed with strong nucleophiles by Sharma and Tomasz (25).

The phase I metabolites, M1–M4, were detected in all three *in vitro* metabolic systems. The dihydroxylation of the methylnaphthyl and indole moieties to give M5 were solely observed in the pHLM incubations for MAM-2201 and the Cl-JWH-122 analogue. M1 and M4 both occurred with high signal intensities after 3 h of incubation with hepatocytes. M2 likewise had high signal intensity, and since it retains the ω-specific characteristics from the parent molecular structure, it is a suitable analytical target for differentiating consumption between the ω-halogenated JWH-122 analogues. Jang *et al.* (22) have previously identified M1 and *N*-4-OH as major JWH-122 targets, and MAM-2201 *N*-4-OH and M4 as targets for MAM-2201. Furthermore, Kong *et al.* confirmed the presence of the MAM-2201 metabolites M1, M2, M3, M4, M5 and M6 after pHLM incubation with the NADPH cofactor (23). Metabolism occurring on the ω-carbon is consistent with this study, although no *N*-4-pentyl-OH metabolites have been observed for any of the investigated compounds in the *in vitro* metabolic systems. *In vivo* detection of metabolites of the aminoalkylindole-type SCRA by Hutter *et al.* furthermore showed that monohydroxylation and/or carboxylation were the main metabolic steps, in line with the findings in the present study (26).

RH and pHH incubations of Cl-, Br- and I-JWH-122 produced the phase II metabolites M7–M9. RH incubations gave rise to identical metabolic pathways when compared with those of the pHH (see Fig. 3), though with different relative amounts (Table I). The ion intensity of the GSH-conjugated metabolite, M9, was higher in RH incubations than in the pHH. The species dependency of this metabolite can be attributed to the amount of glutathione S-transferase in rat hepatocytes compared with that in human hepatocytes (27). When looking at the pHH incubations, the intensity of M9 varied greatly, depending on the parent compound, with M9 originating from I-JWH-122 having the highest signal intensity and Cl-JWH-122 showing the lowest signal intensity after 3 h of incubation in pHH. This is presumably due to iodine being a better leaving group for the S_N2 reaction by the nucleophile sulphur in glutathione. No species-specific metabolites were observed. Relative ion intensities were not assessed in the microsomal studies. MAM-2201 metabolites were previously investigated by Kim *et al.* (2018), who also observed metabolites M1–M8 in mouse, rat and human hepatocytes (21), showing a significant overlap of metabolites of the JWH-122 analogues. In general, metabolite profiling studies of SCRA tend to generate large numbers of metabolites. Due to their relatively high lipophilicity, SCRA have demonstrated high levels of protein binding, which would reduce the free fraction available for metabolism (28,29). As 10% FBS was supplemented to the incubations in this study, less than the 10 μM of the spiked SCRA is available to the suspended hepatocytes. Therefore, only the major metabolites are identified with the experimental set-up used in this study.

Intrinsic Hepatic Stability and Clearance with *In Vitro–In Vivo* Extrapolation

For this study, the quantitative analytical method was applied. The calibrated range for the shared metabolite JWH-122-COOH was between 0.001 (LLOQ) and 3 μM (ULOQ) and between 0.1 (LLOQ) and 3 μM (ULOQ) for JWH-122 and the four ω-halogenated analogues. Accuracy was $< \pm$ 20% for the linear range, while residuals for both calibration ranges were below 20%. The QC performance of the method had a precision and CV% < 20% for all four QC levels for the JWH-122-COOH metabolite and for the three QC levels for

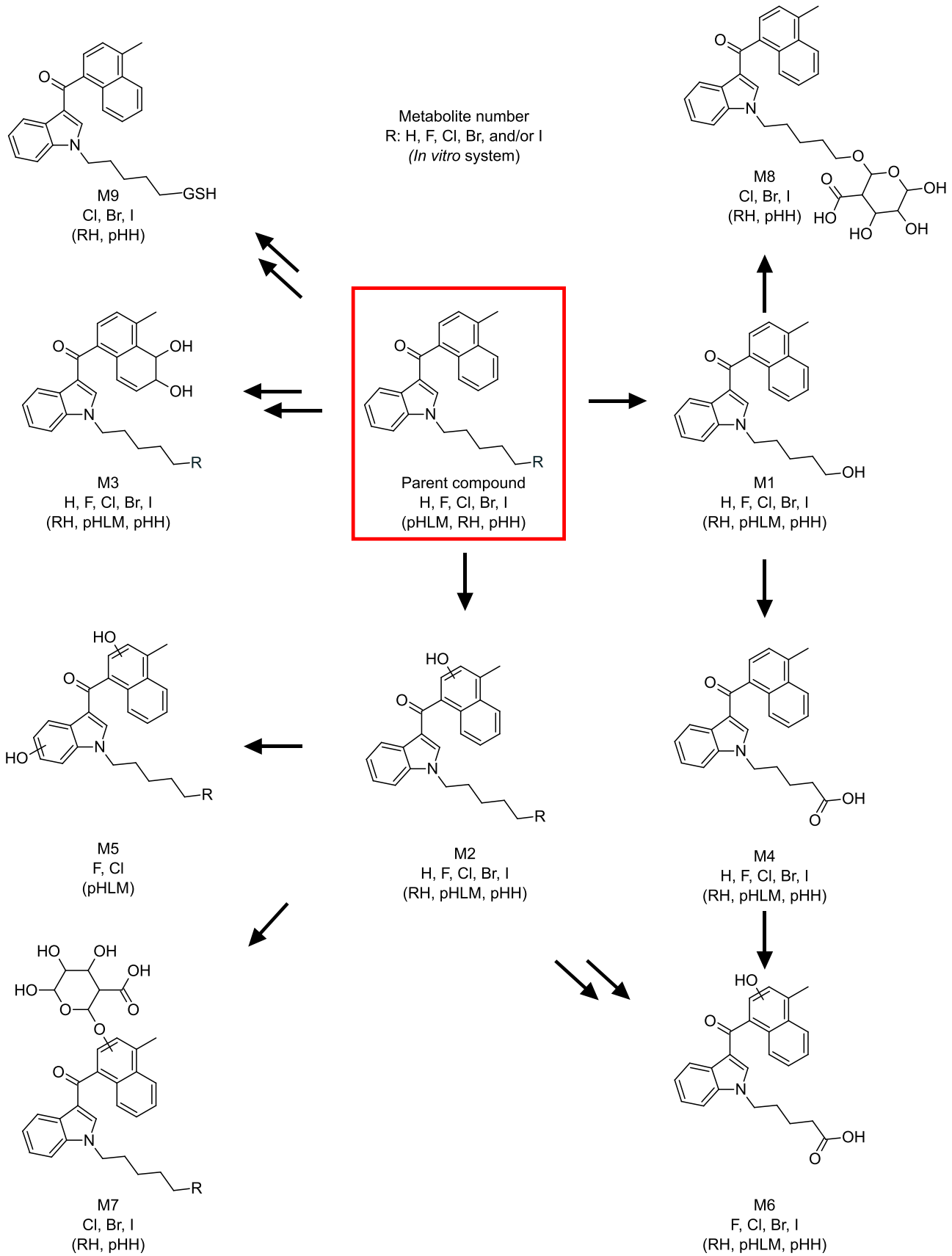

Fig. 3. Proposed metabolic pathway of JWH-122 and its ω-halogenated analogues in microsomes (pHLM), rat hepatocytes (RH) and pooled human hepatocytes (pHH). The R constitutes either hydrogen, fluoro, chloro, bromo or iodo on the ω-carbon

Table II. Comparison of Apparent Intrinsic Clearance ($CL'_{H,int}$) for Five ω-Halogenated JWH-122 Analogues After Incubation with Pooled Human Hepatocytes

Compound	Elimination rate constant, k	$T_{½}$ (min)	$CL'_{H,int}$ (mL/min/kg)
JWH-122	−0.733	0.95	1305
MAM-2201*	−0.791	0.88	1408
Cl-JWH-122	−0.282	2.46	502
Br-JWH-122	−0.279	2.49	497
I-JWH-122	−0.132	5.26	235

*Calculations performed with one data point at LLOQ to acquire linearity in the elimination phase

the five analytes. Carryover was established as < 1% after five consecutive injections of analytes at 3 μM and flushing with solvent.

$CL'_{H,int}$ in hepatocytes for JWH-122 and its ω-halogenated analogues is presented in Table II. The $T_{½}$ for the investigated compounds varied between < 1 and 5 min, with the Cl-, Br- and I-JWH-122 analogues having the highest half-life. Consequently, the lowest $CL'_{H,int}$ was observed for analogues with heavier halogens. The most stable compound was I-JWH-122, followed by Br-JWH-122 and Cl-JWH-122, which showed increasing $CL'_{H,int}$ with decreasing molecular weight. JWH-122 and MAM-2201 both showed a markedly higher $CL'_{H,int}$ at more than fivefold than I-JWH-122. Further scaling was disregarded due to the magnitude of the half-life for the investigated compounds.

The short $T_{½}$ is in accordance with drug user surveys conducted by Winstock and Barratt, who reported consumers of SCRA to have noted a shorter duration of action when compared with natural cannabis (10). The use of hepatocytes for toxicokinetic predictions is a powerful tool when the metabolic pathway is unknown, since non-CYP-mediated reactions are also included in the hepatocyte incubations. A major metabolic step for all compounds was the oxidative dehalogenation. The oxidative dehalogenation of the ω-fluorinated MAM-2201 was investigated in cDNA overexpressed cytochrome enzymes and was mainly mediated by CYP2C8 (23), but also the CYP enzymes 1A2, 2B6, 2C9, 2C18, 2C19, 2D6, 3A4 and 3A5 catalyse the dehalogenation for SCRA (30). Though the metabolic pathway is described for the halogenated MAM-2201, the major metabolic step for the remainder of the halogenated compounds was unknown. This necessitates the use of hepatocytes over the less expensive subcellular fractions to reduce the risk of underpredicting the toxicokinetic parameters (15).

Unspecific binding was accounted for by omitting the first incubation data point at time zero and instead predicting elimination using 30 s as the first time point (18). Assuming that no protein binding occurs *in vivo*, the $CL'_{H,int}$ predictions of the five compounds classify them all as "high clearance drugs". The inclusion of an analytically determined fraction unbound in the medium supplemented with plasma proteins will affect the IVIVE of clearance and will presumably decrease the predicted clearance. This is due to the fact that synthetic cannabinoids are highly lipophilic and therefore more prone to protein binding, which would reduce the amount of free drug available for metabolism (29). This is observed in studies where NPS are detected and quantified *in vivo* several hours after ingestion (3,31,32).

The signal intensity of M1 increased in all compound incubations up to 6 min, followed by a decrease. As illustrated in the proposed metabolic pathway, M1 is an intermediate which can be further metabolised to M8 and M4. Furthermore, the formation rate of the shared metabolite M4 varied depending on the compound of origin. Br- and I-JWH-122 had a fast initial formation rate of the M4 metabolite and were already present at concentrations of around 10-fold higher than LLOQ 30 s after the incubation began. The remaining two halogenated compounds, MAM-2201 and Cl-JWH-122, had similar concentration levels after about 30 min of incubation. JWH-122 showed a markedly lower formation rate of M4 compared with the four halogenated analogues. All halogenated parent compounds generated M4 concentrations between 0.02 and 0.08 μM after a 90 min incubation, while JWH-122 incubation resulted in a 0.002 μM concentration of M4. JWH-122 also had one of the shortest half-lives, but the hepatic stability study indicated the lowest formation rate of the main metabolite M4. The discrepancy is speculated to be a result of ω-oxidative dehalogenation being a faster formation process than ω-hydroxylation, resulting in a lack of the major metabolite for JWH-122. Noble *et al.* (8) and Vigolo *et al.* (7) investigated the *in vitro* and *in vivo* pharmacodynamics of ω-halogenated JWH-122 and JWH-018 analogues, respectively. Both studies found a toxicological effect similar to that of the parent compound, with chloro-halogenated compounds having a higher potency/activity than heavier halogenated analogues. Therefore, the increased $T_{½}$ upon halogenation with higher molecular mass, in combination with similar potency or activity in relation to CB_1 and/or CB_2 receptors, could tend to prolong the time of the effect of SCRA upon ingestion.

CONCLUSION

Based on the metabolite profiling in RH, pHH and pHLM, the following analytical strategies are proposed for Cl-JWH-122, Br-JWH-122 and I-JWH-122: M1 and M4 are proposed as the major analytical targets for consumption, in combination with M2 and M3, to differentiate among JWH-122 analogues. Toxicokinetic studies show a short half-life and thus a high $CL'_{H,int}$ of up to 1305 and 1408 mL/min/kg for JWH-122 and MAM-2201, respectively. The Cl-, Br- and I-JWH-122 showed increasing $T_{½}$ with increasing molecular weight of the ω-halogen, with $CL'_{H,int}$ between 235 and 502 mL/min/kg. Based on this study, ω-halogenation with chloride, bromide or iodide could therefore represent a strategy whereby clandestine drug producers could not only circumvent the local drug legislations but also prolong the duration of action of the SCRA.

ACKNOWLEDGEMENTS

The authors acknowledge Carolina Noble and Niels Bjerre Holm for their support and contribution to this work.

COMPLIANCE WITH ETHICAL STANDARDS

Conflict of Interest The authors declare that they have no conflict of interest.

Ethical Approval This article does not contain any studies with human participants or laboratory animals performed by the authors.

REFERENCES

1. European Monitoring Centre for Drugs and Drug Addiction. Fentanils and synthetic cannabinoids: driving greater complexity into the drug situation. An update from the EU Early Warning System (June 2018). Luxembourg: Publications Office of the European Union; 2018.
2. Saito T, Namera A, Miura N. A fatal case of MAM-2201 poisoning. Forensic Toxicol. 2013;31(2):333–7.
3. Derungs A, Schwaninger AE, Mansella G, Bingisser R, Kraemer T, Liechti ME. Symptoms, toxicities, and analytical results for a patient after smoking herbs containing the novel synthetic cannabinoid MAM-2201. Forensic Toxicol. 2013;31(1):164–71.
4. Roman M, Wu X, Diao X, Josefsson M, Eriksson C, Kugelberg FC, et al. 25C-NBOMe and 25I-NBOMe metabolite studies in human hepatocytes, in vivo mouse and human urine with high-resolution mass spectrometry. Drug Test Anal. 2016;9(5):680–98.
5. Lewin AH, Seltzman HH, Carroll FI, Mascarella SW, Reddy PA. Emergence and properties of spice and bath salts: a medicinal chemistry perspective. Life Sci. 2014;97(1):9–19.
6. Diao X, Wohlfarth A, Pang S, Scheidweiler KB, Huestis MA. High-resolution mass spectrometry for characterizing the metabolism of synthetic cannabinoid THJ-018 and its 5-Fluoro analog THJ-2201 after incubation in human hepatocytes. Clin Chem. 2016;62(1):157–69.
7. Vigolo A, Ossato A, Trapella C, Vincenzi F, Rimondo C, Seri C, et al. Novel halogenated derivates of JWH-018: behavioral and binding studies in mice. Neuropharmacology. 2015;95:68–82.
8. Noble C, Cannaert A, Linnet K, Stove CP. Application of an activity-based receptor bioassay to investigate the in vitro activity of selected indole- and indazole-3-carboxamide-based synthetic cannabinoids at CB1 and CB2 receptors. Drug Test Anal. 2019;11(3):501–11.
9. Cannaert A, Storme J, Franz F, Auwärter V, Stove CP. Detection and activity profiling of synthetic cannabinoids and their metabolites with a newly developed bioassay. Anal Chem. 2016;88(23):11476–85.
10. Winstock AR, Barratt MJ. Synthetic cannabis: a comparison of patterns of use and effect profile with natural cannabis in a large global sample. Drug Alcohol Depend. 2013;131(1–2):106–11.
11. Rane A, Wilkenson GR, Shand DG. Prediction of hepatic extraction ratio from in vitro measurement of intrinsic clearance. J Pharmacol Exp Ther. 1977;200(2):420–4.
12. Gómez-lechón MJ, Tolosa L, Conde I, Donato MT. Competency of different cell models to predict human hepatotoxic drugs. Expert Opin Drug Metab Toxicol. 2014;10(11):1553–68.
13. Castell JV, Jover R, Martnez-Jimnez CP, Gmez-Lechn MJ. Hepatocyte cell lines: their use, scope and limitations in drug metabolism studies. Expert Opin Drug Metab Toxicol. 2006;2(2):183–212.
14. Asha S, Vidyavathi M. Role of human liver microsomes in in vitro metabolism of drugs — a review. Appl Biochem Biotechnol. 2010;160(6):1699–722.
15. Di L, Keefer C, Scott DO, Strelevitz TJ, Chang G, Bi Y-A, et al. Mechanistic insights from comparing intrinsic clearance values between human liver microsomes and hepatocytes to guide drug design. Eur J Med Chem. 2012;57(6):441–8.
16. Noble C, Mardal M, Bjerre Holm N, Stybe Johansen S, Linnet K. In vitro studies on flubromazolam metabolism and detection of its metabolites in authentic forensic samples. Drug Test Anal. 2017;9(8):1182–91.
17. Wohlfarth A, Pang S, Zhu M, Gandhi AS, Scheidweiler KB, Huestis MA. Metabolism of RCS-8, a synthetic cannabinoid with cyclohexyl structure, in human hepatocytes by high-resolution MS. Bioanalysis. 2014;6(9):1187–200.
18. Soars MG, Grime K, Sproston JL, Webborn PJH, Riley RJ. Use of hepatocytes to assess the contribution of hepatic uptake to clearance in vivo. Drug Metab Dispos. 2007;35(6):859–65.
19. Obach RS, Baxter JG, Liston TE, Silber BM, Jones BC, MacIntyre F, et al. The prediction of human pharmacokinetic parameters from preclinical and in vitro metabolism data. J Pharmacol Exp Ther. 1997;283(1):46–58.
20. Poulin P, Haddad S. Toward a new paradigm for the efficient in vitro–in vivo extrapolation of metabolic clearance in humans from hepatocyte data. J Pharm Sci. 2013;102(9):3239–51.
21. Kim J-H, Kong TY, Moon J-Y, Choi KH, Cho Y-Y, Kang HC, et al. Targeted and non-targeted metabolite identification of MAM-2201 in human, mouse, and rat hepatocytes. Drug Test Anal. 2018;10(8):1328–35.
22. Jang M, Shin I, Yang W, Chang H, Yoo HH, Lee J, et al. Determination of major metabolites of MAM-2201 and JWH-122 in in vitro and in vivo studies to distinguish their intake. Forensic Sci Int. 2014;244:85–91.
23. Kong TY, Kim J-H, Choi WG, Lee JY, Kim HS, Kim JY, et al. Metabolic characterization of (1-(5-fluoropentyl)-1H-indol-3-yl)(4-methyl-1-naphthalenyl)-methanone (MAM-2201) using human liver microsomes and cDNA-overexpressed cytochrome P450 enzymes. Anal Bioanal Chem. 2017;409(6):1667–80.
24. Meyer MR, Richter LHJ, Maurer HH. Methylenedioxy designer drugs: mass spectrometric characterization of their glutathione conjugates by means of liquid chromatography-high-resolution mass spectrometry/mass spectrometry and studies on their glutathionyl transferase inhibition potency. Anal Chim Acta. 2014;822:37–50.
25. Sharma M, Tomasz M. Conjugation of glutathione and other thiols with bioreductively activated mitomycin C. Effect of thiols on the reductive activation rate. Chem Res Toxicol. 1994 May;7(3):390–400.
26. Hutter M, Broecker S, Kneisel S, Auwärter V. Identification of the major urinary metabolites in man of seven synthetic cannabinoids of the aminoalkylindole type present as adulterants in 'herbal mixtures' using LC-MS/MS techniques. J Mass Spectrom. 2012;47(1):54–65.
27. Baars AJ, Mukhtar H, Zoetemelk CEM, Jansen M, Breimer DD. Glutathione s-transferase activity in rat and human tissues and organs. Comp Biochem Physiol C Comp Pharmacol. 1981;70(2):285–8.
28. Mardal M, Gracia-Lor E, Leibnitz S, Castiglioni S, Meyer MR. Toxicokinetics of new psychoactive substances: plasma protein binding, metabolic stability, and human phase I metabolism of the synthetic cannabinoid WIN 55,212-2 studied using in vitro tools and LC-HR-MS/MS. Drug Test Anal. 2016;8(10):1039–48.
29. Liu X, Wright M, Hop CECA. Rational use of plasma protein and tissue binding data in drug design. J Med Chem. 2014;57(20):8238–48.
30. Kong TY, Kim J-H, Kim DK, Lee HS. Synthetic cannabinoids are substrates and inhibitors of multiple drug-metabolizing enzymes. Arch Pharm Res. 2018;41(7):691–710.
31. Teske J, Weller J-P, Fieguth A, Rothämel T, Schulz Y, Tröger HD. Sensitive and rapid quantification of the cannabinoid receptor agonist naphthalen-1-yl-(1-pentylindol-3-yl)methanone (JWH-018) in human serum by liquid chromatography–tandem mass spectrometry. J Chromatogr B. 2010;878(27):2659–63.
32. Lonati D, Buscaglia E, Papa P, Valli A, Coccini T, Giampreti A, et al. MAM-2201 (analytically confirmed) intoxication after "synthacaine" consumption. Ann Emerg Med. 2014;64(6):629–32.